Capacity of Multi-Connectivity mmWave Systems with Dynamic Blockage and Directional Antennas

Mikhail Gerasimenko, Dmitri Moltchanov, Margarita Gapeyenko, *Member, IEEE,*
Sergey Andreev, *Senior Member, IEEE* and Yevgeni Koucheryavy, *Senior Member, IEEE*

***Abstract*—The challenges of millimeter-wave (mmWave) radio propagation in dense crowded environments require dynamic re-associations between the available access points (APs) to reduce the chances of losing the line-of-sight (LoS) path. However, the antenna beamsearching functionality in the mmWave systems may introduce significant delays in the course of AP re-association. In this work, we analyze user performance in dense urban mmWave deployments that are susceptible to blockage by the dynamically moving crowd. Our approach relies on the ergodic capacity as the key parameter of interest. We conduct a detailed evaluation with respect to the impact of various system parameters on the ergodic capacity, such as AP density and height, blocker density and speed, number of antenna array elements, array switching time, degree of multi-connectivity, and employed connectivity strategies. Particularly, we demonstrate that dual connectivity delivers the desired performance out of all possible degrees of multi-connectivity, and there is an optimal density of mmWave APs that maximizes the capacity of cell-edge users. We also show that the use of low complexity "reactive" multi-connectivity design, where the beamtracking is only performed when the currently active connection is lost, together with the utilization of iterative beamsearching algorithms, does not significantly deteriorate the ergodic capacity.**

I. Introduction

Millimeter-wave (mmWave) communications technology is expected to provide the basis for fifth-generation (5G) mobile networks that enable extremely high data rates and low latencies at the air interface [1], [2]. While 3GPP's standardization process on mmWave-ready New Radio (NR) is almost complete and vendors are performing test trials to showcase the capabilities of this emerging system design, researchers continue exploring the challenges related to enabling advanced networking options for 5G [3], [4].

In contrast to legacy microwave systems, where base station re-associations are primarily caused by the mobility of a user and thus do not occur as often, the specifics of mmWave propagation may call for much more frequent cell changes. Indeed, even when the active user is static, the movements of other nearby objects, such as humans and vehicles, may cause line-of-sight (LoS) blockage. This, in turn, leads to a rapid degradation in the received signal strength that could result in unwanted outages [5]. This problem is aggravated by the fact that blocked period durations are expected to be hundreds of milliseconds [6].

One of the possible solutions to improve mmWave coverage is to use beamforming [7]. However, beamforming efficiency highly depends on the number of array elements and the specifics of beamsearching algorithms, user equipment (UE) misdetection and discovery delays [8], propagation conditions (indoor vs. outdoor), and likelihood of channel variations (interference, direction of arrival, etc.) [9]. To improve beamsearching speed and efficiency, it is possible to utilize location information [10] and other network assistance functions [11], which can bring additional benefits to 5G heterogeneous networks (HetNets) [12], [13].

Despite the fact that beamforming improves mmWave coverage, it does not significantly increase performance in case of human body blockage. To ensure user session continuity in dense mmWave deployments, multi-connectivity techniques have recently been proposed by 3GPP [14]. This approach relies on simultaneous active connections to multiple access points (APs). Even though only one of these might be used at a time, multi-connectivity may efficiently combat outages by enabling backup connections whenever needed [15]. However, practical implementation of multi-connectivity schemes is expected to add considerable overheads on physical and medium access control layers at both the UE and the AP.

To support a backup mmWave connection, the UE needs to (i) acquire a beacon signal from the AP by using omnidirectional antenna mode, (ii) perform AP association procedure (e.g., via a random-access scheme), and (iii) begin tracking the AP beam, such that fast switching is possible in case of LoS blockage [16]. While the first two procedures need to be performed only once, the latter has to be invoked repeatedly to keep the backup link active. The time interval between the beamtracking updates depends on many parameters, including user mobility and beamwidth, and can be configured to several microseconds [17]. This places an extreme computational burden on the UE side, especially when the number of backup connections is higher than one [18].

In this paper, we propose and analyze "reactive" mmWave multi-connectivity operation, where the beamtracking for backup APs is performed on-demand, only when the currently active connection is lost. This approach may lead to a much more "lightweight" solution in terms of hardware and software implementation – potentially allowing to support more backup connections to further reduce outage times. At the same time, such reactive nature of the proposed approach may lead to outages when the beamsearching procedure is just initiated. Concentrating on the UE that experiences an outage in its blocked state and assuming dense mmWave AP deployment

M. Gerasimenko, D. Moltchanov, M. Gapeyenko, and S. Andreev are with the Laboratory of Electronics and Communications Engineering, Tampere University of Technology, Tampere, Finland (e-mail: firstname.lastname@tut.fi), Y. Koucheryavy is with the Laboratory of Electronics and Communications Engineering, Tampere University of Technology, Tampere, Finland and National Research Institute Higher School of Economics, Moscow, Russia (e-mail: evgeni.kucheryavy@tut.fi)

with a moving crowd, we analyze several mmWave connectivity options, including static and dynamic operation.

The main contributions of this work are:

- a mathematical framework for ergodic capacity analysis of cell-edge users in mmWave deployments with directional antenna arrays and multi-connectivity capabilities in dynamic blockage-prone environments;
- an investigation of the effects of system parameters on ergodic capacity, including mmWave AP density and height, density and speed of blockers, number of antenna array elements, array switching time, degree of multi-connectivity, and connectivity strategies;
- a numerical analysis of reactive multi-connectivity operation with exhaustive and iterative beamsearching algorithms, where beamsearching is performed only when the currently active connection is lost;
- a numerical illustration of the fact that dual connectivity delivers the desired performance out of all possible degrees of multi-connectivity, and there is an optimal density of mmWave APs that maximizes the capacity of cell-edge users.

The rest of this text is organized as follows. Related work is covered in Section II. We introduce our system model and the considered multi-connectivity schemes in Section III. The theoretical framework for ergodic capacity evaluation is developed in Section IV. Numerical analysis is provided in Section V. Conclusions are drawn in the last section.

II. Related Work

The initial research works on mmWave communications concentrated on developing theoretical tools to capture the intricate specifics of such systems, such as highly directional transmission, path blockage, and atmospheric absorption. Applying the Campbell theorem for functionals over point processes, the moments of aggregate interference in THz and mmWave systems in presence of molecular absorption, human-body blockage, and directional transmit and receive antennas have been derived in [19]. Using the Taylor expansion approximation, the authors then extended their analysis to the moments of signal-to-interference ratio (SIR) in [20].

Deriving distributions of aggregate interference and SIR is a more challenging task. Several research groups have recently adopted a microwave propagation model in the form of $P_R(x) = Ax^{-\gamma}$ for the performance analysis of mmWave communications technology, see, e.g., [21], [22]. Particularly, the authors in [21] obtained the probability density function (PDF) of SIR for mmWave systems operating at 28 GHz. The PDFs of interference and SIR in the absence of blockage have been reported in [23]. The SIR distribution is further contributed by [24], where the authors introduced a simple model of atmospheric absorption that assumes a constant attenuation coefficient as well as disregards the effect of blockage.

Later on, by relying on the developed theoretical methods, mmWave research focused on revealing practical insights into system-level performance. Assessing the hypothesis of noise-limited operation in 5G mmWave systems [25], the authors in [26] developed an analytical framework for characterizing throughput performance as a function of the AP density. It was demonstrated that there is an optimal density of the APs that maximizes the system throughput for a given SINR threshold. Further, in [27], the authors proposed to employ partial zero forcing at the UE side to cancel out the interference from the APs. They also derived the probability of coverage with directional antennas at both the UE and the AP sides.

Most of the papers studying multi-connectivity focus on a joint operation of the mmWave RAT and conventional cellular network by concentrating on higher-layer integration and overall multi-RAT architecture design [28]. While it becomes clear that offloaded control signaling to the below-6GHz networks provides more flexibility in terms of user mobility and connection reliability [29], there are only a few studies that address the aspects of simultaneous/alternate multi-AP mmWave user connectivity strategies. Employing computer simulations, the authors in [30] demonstrated that in presence of static blockage by buildings the use of multi-connectivity may drastically improve performance of mmWave systems in terms of session reliability.

In [31], the authors assessed the performance of mmWave systems by using several hard handover algorithms, including rate-based, load-based, traditional SNR-based, and novel Markov Decision Process (MDP)-based solutions. However, the emphasis of that work is mainly on system-level performance indicators. Another interesting example of mmWave handover is presented in [32], where the authors proposed to use RGB-D cameras to improve performance by predicting possible human body blockage. On the other hand, the analytical model presented by the authors is limited to the "two APs" scenario and does not allow to capture the effects of dense deployments as well as varying blocker/AP densities on the system scale.

Finally, the authors in [14] considered the performance of dynamic multi-connectivity in urban deployment by using a mixture of ray-tracing computer simulations, queuing theory, and stochastic geometry. However, the modeling framework proposed therein cannot be extended to the case of arbitrary degree of multi-connectivity. Despite several attempts to incorporate the peculiarities of mmWave communications into analytically tractable frameworks, to the best of our knowledge, this is the first work that analytically embraces the main features of mmWave technology, such as directional antennas and dynamic human body blockage, to evaluate its system-level performance with multi-connectivity operation.

III. System Model

In this section, we introduce our system model. We begin by describing the target deployment, mobility, and blockage models. Then, propagation, antenna, and beamforming components are detailed. Finally, connectivity strategies and metrics of interest are specified. The notations used in the remainder of this paper are summarized in Table I.

A. Deployment Model

We assume that locations of mmWave APs follow a Poisson point process (PPP) in $\Re^2$ with a certain intensity of λ_A, see

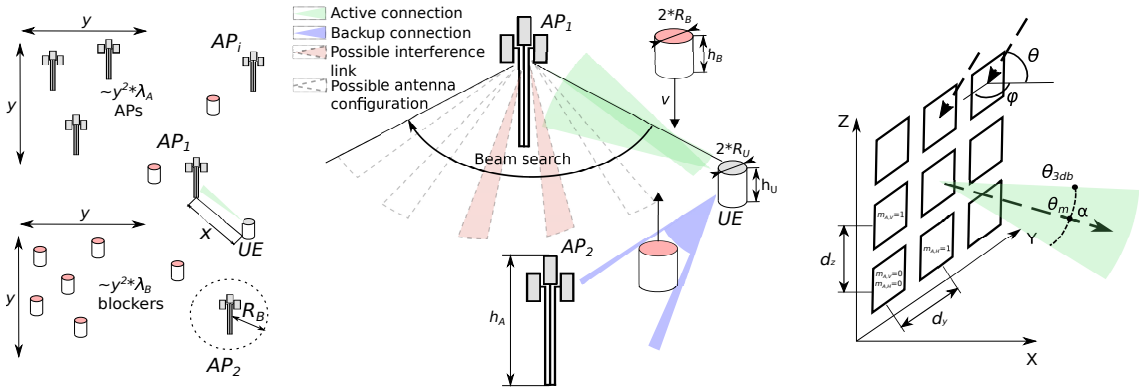

Fig. 1. An illustration of elements that comprise our system model.

Fig. 1(a). This assumption is in-line with the recent studies of dense AP deployments [33], [34]. The height of APs is assumed to be fixed and set to h_A, see Fig. 1(b).

In our study, we concentrate on the performance of a tagged user that is assumed to be stationary. The height of the UE is constant, h_U. We further assume that the moving crowd in the area of interest acts as potential blockers to the tagged user. The spatial intensity of blockers is constant, λ_B, as they move according to a certain mobility model. In this work, we consider the random direction model (RDM) [35] as the one capturing the essentials of random movement and still preserving analytical tractability. According to RDM, a blocker first randomly chooses its movement direction uniformly in $(0, 2\pi)$ and then travels in this direction for an exponentially distributed interval of time with the parameter $\nu_B = 1/E[\tau_B]$, where τ_B is the mean duration of the movement. The moving speed is assumed to be constant, v_B. By selecting values of (ν_B, v_B), one can represent crowds with different densities.

To capture the LoS blockage dynamics, we impose that the radius of human blockers is constant and equals to r_B. The height of blockers is different from that of the UE and is set to h_B, $h_B > h_U$. Whenever such blockers cross the direct path between the tagged user and its serving AP, the LoS mmWave path is assumed to be blocked.

B. Propagation Model

For any density of mmWave APs, λ_A, we concentrate on the cell-edge UE that is located farther away than a certain distance of R_B from the nearest AP, where the blockage leads to outage, since the signal strength of multipath components is below the required level. Hence, the terms of blockage and outage are used interchangeably in what follows. The distance R_B may be obtained by using the propagation model introduced below and interference is evaluated in Section IV.

The received signal power at the UE can be written as

$$P_R(x) = P_T G_T G_R A x^{-\gamma}, \tag{1}$$

where P_T is the transmit power, G_T and G_R are the antenna gains at the transmit and receive sides, respectively, which depend on the antenna array, x is the distance between the UE and the AP, A and γ are the propagation coefficients.

In this paper, we do not consider the non-LoS (NLoS) state (blockage by large objects, such as buildings) by assuming an open-space scenario, where there are no massive obstacles. However, we account for blockage of the LoS signal path by human bodies. Following [36], the mmWave path loss in dB is given by

$$L(x) = 20\log_{10}(4\pi/\lambda) + 21\log_{10}(x) + 4.9, \tag{2}$$

where λ is the wavelength and x is the three-dimensional distance between the UE and the AP.

Therefore, the coefficients A and γ are

$$A = 10^{-2\log_{10}(\pi/\lambda_0)+0.49}, \quad \gamma = 2.1. \tag{3}$$

C. Beamforming and Antenna Models

To complete the parametrization of the propagation model, one requires antenna gains G_T and G_R. In this paper, we assume linear antenna arrays at both the transmit and receive sides. Following [37], the antenna factor is defined as

$$AF(\theta, \beta) = \frac{\sin(N[\pi\cos(\theta) + \beta]/2)}{\sin([\pi\cos(\theta) + \beta]/2)}, \tag{4}$$

where N is the total number of elements in an array, β specifies the direction of the array, and θ is the azimuth angle. In what follows, we assume $\beta = 0$ and the distance between the neighboring elements to be $\lambda/2$, where λ is the wavelength.

We model the radiation pattern of an antenna array by using the cone model [38]. The directivity of the mmWave AP's transmit antenna is represented as a conical zone with the angle of α_T, as shown in Fig. 2. This model is an abstraction assuming no side lobes and constant power at a

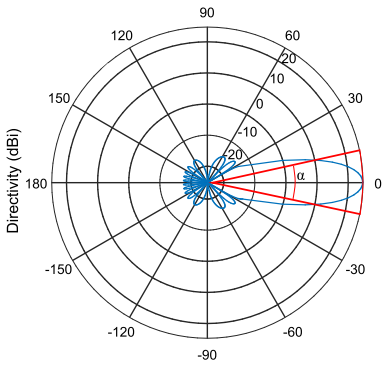

Fig. 2. Cone antenna radiation pattern model.

TABLE I
NOTATION USED IN THIS PAPER.

Parameter	Definition
λ_A	Spatial density of mmWave APs
h_A	Height of mmWave APs
λ_B	Spatial density of blockers
h_U	Height of UE devices
h_B	Height of blockers
r_B	Radius of blockers
R_B	Distance at which blockage leads to outage
$E[\tau_B]$	Mean single run-time in RDM model
ν_B	Intensity of single runs in RDM
v_B	Speed of blockers
P_T	AP transmit power
$P_R(x)$	Received power at distance x
$L(x)$	Path loss at distance x
G_T, G_R	Antenna gains at transmit (AP) and receive (UE) sides
λ	Wavelength
γ	Path loss exponent
A	Propagation coefficient
$AF(\theta,\beta)$	Array factor
β	Array direction angle
θ	Azimuth array angle
α_T, α_R	Transmit (AP) and receive (UE) antenna directivities
δ	Antenna array switching time
T_S	Beamsearching time
N_U, N_A	Number of horizontal antenna elements at UE and AP
N	Degree of multi-connectivity
C	Ergodic capacity
B	Available bandwidth
$S, S(t)$	SIR of a user
c	A constant to account for MCS imperfections
$d(x), S_B(x)$	Length and area of blockage zone
$p_L(x)$	Non-blockage probability at distance x
$f_i(x), f_i(x;y)$	Distance and conditional distance to i-th nearest AP
$p_{L,i}$	Non-blockage probability with i-th nearest AP
$\zeta(x)$	Temporal intensity of a single blocker at distance x
$\mu_B(x)$	Temporal intensity of blockers at distance x
$f_{D_1}(l;x), f_{D_2}(l;x)$	pdfs of distances traveled in LoS blockage zone
w_1, w_2	Weighting coefficients
$f_T(t;x)$	pdf of time spent in LoS blockage zone at distance x
$F_L(t;x), F_B(t;x)$	CDF of non-blockage/blockage time at distance x
$f_{L,i}(t), f_{B,i}(t)$	pdfs of blockage/non-blockage time with AP i
$E[R_i]$	UE capacity when connected to i-th nearest AP
N_0	Noise power at 1Hz
$P_{R,i}$	Received power from i-th nearest AP
$E[I^n]$	n-th moment of aggregate interference
$p_C(x)$	Probability of required antenna orientation
R_I	Non-negligible interference radius
w_i	Probability that L_i is greater than T_S
$f_{A,i}(x)$	Active time conditional pdf when connected to AP i
$p_{A,i}$	Fraction of time that link is active
q_i	Association probability with i-th nearest AP
u_{ij}	Transition probabilities of Markov model for $N=\infty$
$\vec{\pi}$	Steady-state probabilities of Markov model for $N=\infty$
$\vec{e}$	Vector of ones with appropriate size
T_1	Uninterrupted period when there is non-blocked AP available
T_2	Uninterrupted period when no non-blocked APs are available
B_i^*	Residual blockage time
a_i	Probability that T_1 ends with i-th nearest AP
$\vec{u}$	Absorption probabilities of Markov model for fixed N
D	Fundamental matrix of absorbing Markov model for fixed N
b_i	Probability that T_1 starts with i-th nearest AP

certain separation distance from the transmitter. The directivity of the receiver is modeled by imposing constant sensitivity of the antenna in the direction of α_R.

The crucial coefficients of the antenna model – transmit and receive directivities α_T and α_R – need to be related to the parameters of the antenna arrays. Half-power beamwidth (HPBW) of the array, α, is proportional to the number of elements in the appropriate plane and could be established as

$$\alpha = 2|\theta_m - \theta_{3db}|, \tag{5}$$

TABLE II
ANTENNA HPBW AND ITS APPROXIMATION

Array	Value, direct calculation	Approximation
64x1	1.585	1.594
32x1	3.171	3.188
16x1	6.345	6.375
8x1	12.71	12.75

where θ_{3db} is the 3-dB point and θ_m is the location of the array maximum. The latter is computed as

$$\theta_m = \arccos(-\beta/\pi). \tag{6}$$

Assuming $\beta = 0$, we have $\theta_m = \pi/2$. The upper and lower 3-dB points are thus

$$\theta_{3db}^{\pm} = \arccos[-\beta \pm 2.782/(N\pi)]. \tag{7}$$

Accordingly, Table II demonstrates the antenna array HPBW and its approximation by using $102/M$, where M is the number of array elements. For $\beta = 0$, the mean antenna gain over HPBW is then [37]

$$G = \frac{1}{\theta_{3db}^{+} - \theta_{3db}^{-}} \int_{\theta_{3db}^{-}}^{\theta_{3db}^{+}} \frac{\sin(N\pi\cos(\theta)/2)}{\sin(\pi\cos(\theta)/2)} d\theta. \tag{8}$$

The antenna gains are summarized in Table III.

D. Beamsearching Algorithms

We consider two beamsearching algorithms:

- *Exhaustive search.* In this case, the most beneficial configuration from the signal strength perspective is established by attempting all the available configurations at both the AP and the UE. The time complexity of this approach is $T_S = N_U N_A \delta$, where N_U and N_A are the numbers of possible UE and AP antenna array configurations and δ is the switching time.
- *Iterative search.* As an alternative, we consider iterative beamsearching realized with sector level sweep and beam refinement procedures. This solution is used in, e.g., [39], where Rx and Tx perform beamsearching separately by forcing the other side to use the omnidirectional mode. Particularly, the Tx side sends beacon packets through all possible array configurations, while the Rx measures the received signal strength in the omnidirectional mode. At the second step, these roles are inverted. The time complexity here is $T_S = (N_U + N_A)\delta$.

The array switching time, δ, is a key parameter that depends on the implementation and may vary from microseconds to milliseconds. For example, in IEEE 802.11ad (WiGig), δ is defined as Short Beamforming Interframe Space (SBIFS) with the default value of 1ms [39]. Here, assuming the typical

TABLE III
ANTENNA ARRAY GAINS

Array	Gain, linear	Gain, dB
64x1	57.51	17.59
32x1	28.76	14.58
16x1	14.38	11.57
8x1	7.20	8.57
4x1	3.61	5.57

values of $N_A = 64$ and $N_U = 4$, T_S is 4ms and 0.41ms for exhaustive and iterative search, respectively.

In addition to exhaustive and iterative techniques, there is a number of hierarchical algorithms [40]. In hierarchical search, the antenna array codebooks specify not only different beam directivity options but also several beamwidth configurations. When sweeping procedure starts, the array is initially locked to the configuration with the widest beamwidth. When the widest beam configuration is found, the array is switched to the lower "layer" by performing an iterative search in the direction of the established solution. The complexity of hierarchical search depends on the number of beamwidth "layers", having the minimum complexity of $O(\log_2(N))$ for $\log_2(N)$ layers.

E. Connectivity Strategies and Metrics

We assume that whenever the UE utilizes an active connection to a certain mmWave AP, it maintains backup connections to a number of other APs in the area, thus alleviating the need for channel access procedures. We consider the following connectivity schemes:

- *Static, nearest AP*. In this scheme, the UE is associated with its nearest AP. Note that due to the convexity of the propagation model, this scheme provides the best possible conditions in the non-blocked state. In practice, this scheme is implemented by associating with the AP having the best average signal-to-noise ratio (SNR).
- *Static, LoS.* In this scheme, upon its session initiation, the UE selects an AP with the best current SNR. Note that due to random distances to the APs as well as random blockage states w.r.t. these APs, the selected AP may not be the closest one providing the best possible conditions in the non-blocked state. In practice, this scheme is implemented by associating with the AP having the best instantaneous SNR.
- *Dynamic, finite N*. In this scheme, the UE changes its association point whenever it enters the blockage state with the current AP. At both session initiation and re-association time instants, the closest non-blocked AP out of the nearest N is chosen.
- *Dynamic, $N = \infty$.* In this scheme, the UE also changes its association point choosing the nearest non-blocked AP whenever it enters the blockage state with the current AP. However, the number of APs that it may associate with is unlimited.

For the considered system model, we are interested in the downlink performance, that is, from the AP to the UE. Our parameter of interest is the ergodic capacity defined as

$$C = \lim_{t\to\infty} \frac{1}{t} \int_0^t cB\log[1+S(t)], \tag{9}$$

where B is the bandwidth requested by the user from the APs that it is associated with, $S(t)$ is the signal-to-interference-plus-noise ratio (SINR) at the UE, and c is a constant that accounts for any modulation and coding scheme (MCS) imperfections.

IV. Performance Evaluation Framework

In this section, we develop a mathematical framework for the performance evaluation of the introduced mmWave connectivity strategies by utilizing the ergodic capacity as our metric of interest. We begin by describing the framework and then proceed with specifying the sub-models.

A. Framework at a Glance

Our proposed framework comprises three logical steps: (i) modeling the blockage dynamics by a randomly moving crowd for the UE of interest, (ii) specifying the capacity model with i-th nearest AP, and (iii) extending the said models with the multi-connectivity operation and deriving the ergodic capacity.

First, the following subsection specifies the dynamics of the LoS blockage process between the mmWave APs and the UE. We determine the ergodic probabilities, p_i, $i = 1,2,\ldots$, when the LoS path to the i-th nearest mmWave AP in the spatial process of APs is blocked. These probabilities are further used to characterize the best available AP at a random instant of time. We also show that for the realistic densities of APs, the LoS paths to the first several APs can be considered independent. Further, we characterize the dynamics of the mmWave AP associations and arrive at the process that captures the time intervals of having the LoS path blocked or unblocked with i-th nearest mmWave AP. These results are employed to determine the UE throughput received from the mmWave APs.

The use of larger numbers of antenna elements at both the mmWave AP and the UE increases the beamsearching time, thus decreasing the available association time with the mmWave AP when the multi-connectivity operation is enabled. On the other hand, this induces better antenna directivity and hence may improve the received signal strength – by increasing capacity during the association time. To characterize the channel capacity when associated with i-th AP, at the second step, we develop interference, SINR, and capacity models that describe these metrics.

At the last step, we combine our blockage and capacity models as well as supplement them with the multi-connectivity strategies to obtain the ergodic capacity made available to the UE. The said capacity is expressed as a function of the densities of spatial blockers and mmWave APs, the mobility parameters of blockers, the number of antenna elements used for beamsearching, and the type of connectivity strategy in use, thus facilitating further numerical assessment.

B. Blockage Process Dynamics

Consider the process of LoS blockage by moving human bodies around the stationary UE located at the two-dimensional distance x from the mmWave AP, see Fig. 3. There always is some area, where the presence of at least a single blocker causes the blockage of the LoS path between the AP and the user. We refer to this area as to *LoS blockage zone*. For the realistic distances between the UE and the AP, the area of the LoS blockage zone can be approximated by a rectangle. The sides of this zone are $2r_B$ and

$$d(x) = x\frac{h_B - h_U}{h_A - h_U} + r_B. \tag{11}$$

The area of the LoS blockage zone is thus

$$S_B(x) = 2r_B d(x) = 2r_B\left(x\frac{h_B - h_U}{h_A - h_U} + r_B\right). \tag{12}$$

$$p_{L,i} = \frac{1}{(i-1)!}\Gamma(i)\,{}_1F_1\left(i;\frac{1}{2};\frac{(h_U r_B\lambda_B - h_B r_B\lambda_B)^2}{(h_A-h_U)^2\pi\lambda_A}\right) + \frac{2\lambda_B r_B(h_U-h_B)\Gamma\left(i+\frac{1}{2}\right)\,{}_1F_1\left(i+\frac{1}{2};\frac{3}{2};\frac{(h_U r_B\lambda_B - h_B r_B\lambda_B)^2}{(h_A-h_U)^2\pi\lambda_A}\right)}{\sqrt{\pi}\sqrt{\lambda_A}(h_A-h_U)(i-1)!}. \quad (10)$$

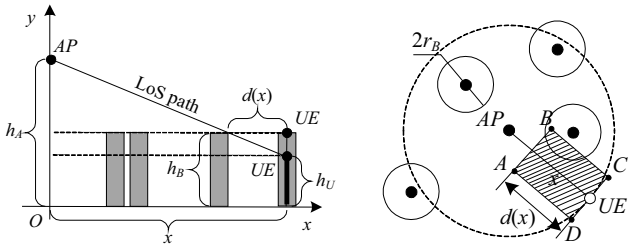

(a) Side view (b) Top view

Fig. 3. Configuration of the LoS blockage zone.

The limiting pdf of blocker locations as they move within a certain bounded area in $\Re^2$ according to the RDM is uniform [35]. Hence, at any given instant of time t the positions of blockers form a PPP with the spatial intensity of λ_B. The probability that the LoS path is not blocked corresponds to the void probability of the Poison process of blockers, that is

$$p_L(x) = \exp\left(-2\lambda_B r_B\left[x\frac{h_B-h_U}{h_A-h_U}+r_B\right]\right). \quad (13)$$

The pdf of distance to i-th neighbor in the Poisson field of mmWave APs is available from [41]

$$f_i(x) = \frac{2(\pi\lambda)^i}{(i-1)!}x^{2i-1}e^{-\pi\lambda x^2}, x>0, i=1,2,\ldots. \quad (14)$$

Recall that we consider the UE that is located farther away than R_B from its nearest AP. The conditional pdf of distance to i-th AP, given that it is greater than y, is produced by

$$f_i(x;y) = \frac{2(\pi\lambda_A)^i}{\Gamma(i,\pi y^2\lambda_A)}x^{2i-1}e^{-\pi\lambda_A x^2}, x>y, i=1,2,\ldots, \quad (15)$$

where $\Gamma(a,x)$ is incomplete Gamma function,

$$\Gamma(a,x) = -\int_x^\infty t^{a-1}e^{-t}dt. \quad (16)$$

Hence, the non-blockage probability to i-th mmWave AP is

$$p_{L,i} = \int_{R_B}^\infty \frac{2(\pi\lambda_A)^i}{\Gamma(i,\pi R_B^2\lambda_A)}x^{2i-1}e^{-\pi\lambda_A x^2}e^{-2xr_B\lambda_B\frac{h_B-h_U}{h_A-h_U}}dx, \quad (17)$$

thus leading to (10) where $\Gamma(x)$ is the Gamma function,

$$\Gamma(x) = \int_0^\infty t^{x-1}e^{-t}dt, \quad (18)$$

and ${}_1F_1(a,b,x)$ is Kummer hypergeometric function,

$${}_1F_1(a,b,x) = \sum_{k=0}^\infty \frac{a^{(k)}}{b^{(k)}}\frac{x^k}{k!}, \quad (19)$$

where $a^{(0)}=1$ and $a^{(k)} = a(a+1)(a+2)\ldots(a+n-1)$.

The probability $p_{L,i}$ can be interpreted as a fraction of time that i-th mmWave AP resides in the non-blocked state. In addition to these probabilities, we also require the knowledge of the time interval for i-th mmWave AP to remain in blocked/non-blocked state. As opposed to the time-averaged analysis, we now need to explicitly track blocker dynamics as they cross the LoS blockage zone.

To capture blockage dynamics, one has to determine the temporal intensity of blockers, $\mu_B(x)$, which enter the LoS blockage zone associated with the UE located at the distance of x. It has been shown in [42] that the inter-meeting time between two users with circular coverage areas of their transceivers having the radii of r and moving according to the RDM within the area of $W\subset\Re^2$ with random speeds of V_1 and V_2 follows an exponential distribution with the parameter

$$\zeta = 2rE[V]\int_W f^2(x,y)dxdy, \quad (20)$$

where $E[V]$ is the mean relative speed of users and $f(x,y)$ is the stationary distribution of the RDM in W.

In our case, the speed of a user is constant, v, while the speed of the LoS blockage zone is zero, thus implying that $E[V]=v_B$. Further, the density of blockers, λ_B, is constant in $\Re^2$, which yields that one can choose W to be, e.g., a square with the side of R, fully containing the LoS blockage zone. Therefore, the intensity of meetings of a single blocker with the LoS blockage zone associated with the UE located at the distance of x is

$$\zeta(x) = 2r_B v_B\left(x\frac{h_B-h_U}{h_A-h_U}+r_B\right)\int_0^R\int_0^R f^2(x,y)dxdy = \\ = \frac{2r_B v_B(x[h_B-h_U]+r_B[h_A-h_U])}{R^2(h_A-h_U)}, \quad (21)$$

where $f(x,y)=1/R^2$ is the stationary pdf of the RDM [35].

The number of blockers falling into the square with the side of R follows a Poisson distribution with the mean of $\lambda_B R^2$. Applying the superposition property of the Poisson process, the spatial intensity of blockers is related to the temporal intensity of blockers as

$$\mu_B(x) = \frac{2r_B\lambda_B v_B(x[h_B-h_U]+r_B[h_A-h_U])}{(h_A-h_U)}. \quad (22)$$

Since the time between when the blockers enter the LoS blockage zone is distributed exponentially, the process of how the blockers enter this zone is homogeneous Poisson with the intensity of $\mu_B(x)$. Note that due to the properties of the RDM model the entry point of an arbitrary blocker is distributed uniformly over the perimeter of the LoS blockage zone.

Observe that the blockage process forms an alternating renewal process [6]. Let B and L be the random variables (RVs) that denote the blocked and non-blocked periods, respectively. Since blockers enter the zone according to a Poisson process, the time spent in the non-blocked period, L, follows an exponential distribution with $\mu_B(x)$, $F_L(t;x) = 1-e^{-\mu_B(x)t}$, where x is the parameter. Indeed, since the inter-entry times are exponential, the distance from the end of the blocked part – considered as an arbitrary point – to the starting point of the next blocked interval is distributed exponentially [43].

$$E[R_i] \approx \frac{\mu_P}{N_0+\mu_I} + \frac{cB\mu_P\sigma_I^2}{(N_0+\mu_I)^3\left(1+\frac{\mu_P}{N_0+\mu_I}\right)} - \frac{cB\mu_P^2\sigma_I^2}{2(N_0+\mu_I)^4\left(1+\frac{\mu_P}{N_0+\mu_I}\right)^2} - \frac{cB\sigma_P^2}{(N_0+\mu_I)^2\left(1+\frac{\mu_P}{N_0+\mu_I}\right)^2}. \quad (23)$$

Further, consider the blocked interval. Let T be the RV that denotes the residence time in the LoS blockage zone for a single blocker and let $f_T(t;x)$ be its pdf. We determine the pdf of the distance traveled by a blocker within the LoS blockage zone, $f_D(l;x)$, and then scale it with the constant velocity of v_B. Using the notion of geometric probability arguments, the pdf $f_D(l;x)$ is delivered by

$$f_D(l;x) = \frac{f_{L_1}(l;x)}{w_1^{-1}} + \frac{f_{L_2}(l;x)}{w_2^{-1}}, 0 < t \le \sqrt{d^2(x)+4r_B^2}, \quad (24)$$

where the pdfs $f_{L_1}(t;x)$ and $f_{L_2}(t;x)$ are produced by

$$f_{D_1}(l;x) = \begin{cases} 0, & l \le 0, \\ \pi l/4d(x)r_B, & 0 < l \le l_1, \\ l\sin^{-1}\left(\frac{m_1}{l}\right)/2d(x)r_B, & l_1 < l \le l_2, \\ \frac{l\sin^{-1}\left(\frac{2r_B}{l}\right) - l\cos^{-1}\left(\frac{d(x)}{l}\right)}{2d(x)r_B}, & l_2 < l \le l_3, \end{cases}$$
$$f_{D_2}(l;x) = \begin{cases} 0, & l \le 2r_B, \\ \frac{2l}{d^2(x)}\left(\frac{d(x)}{\sqrt{l^2-4r_B^2}} - 1\right), & 2r_B < l \le l_3, \end{cases} \quad (25)$$

with the limits of

$$\begin{cases} l_1 = \min[2r_B, d(x)], \\ l_2 = \max[2r_B, d(x)], \\ l_3 = \sqrt{d^2(x)+4r_B^2}, \end{cases} \quad (26)$$

while the weights w_1 and w_2 denote (i) the probability for a blocker to start from the side of length $d(x)$ and end at the side of length $2r_B$ (or vice versa), and (ii) the probability for a blocker to start from the side of length $d(x)$ and end on the other side of length $d(x)$. These probabilities are calculated as

$$w_1 = \frac{d^2(x)+6d(x)r_B}{d^2(x)+2d(x)r_B+8r_B^2}, \quad w_2 = \frac{8r_B^2}{d^2(x)+6d(x)r_B+8r_B^2}. \quad (27)$$

The pdf of the residence time in the LoS blockage zone can now be obtained by the linear transformation L/v_B, where v_B is the speed of blockers. Recall that the density of linear transformation $Y = a+bX$ is given by [44]

$$f_Y(y) = f_X[g^{-1}(y)]\left|\frac{dx}{dy}\right| = f_X\left(\frac{y-a}{b}\right)\frac{1}{|b|}, \quad (28)$$

thus implying that the pdf of $T = L/v_B$ is

$$f_T(t;x) = f_D(vt;x)v. \quad (29)$$

Let $F_B(t;x)$ be the cumulative distribution function (CDF) of the blocked interval. The distribution of the blocked interval is the same as that of the busy period in $M/GI/\infty$ system [6],

$$F_B(t;x) = 1 - \Bigg(\int_0^t (1-F_B(t-z;x))|de^{-\zeta(x)F_T(z;x)}| - \\ - [1-F_T(t;x)]\int_0^t [1-F_B(t-z;x)]e^{-\zeta(x)F_T(z;x)}\zeta dz + \\ + [1-F_T(t;x)]\Bigg). \quad (30)$$

Observe that the LoS blockage processes at various APs are approximately independent of each other, as dependence appears only due to an overlap of the LoS blockage zones across different APs. For the realistic mmWave deployments, these areas are relatively small as compared to the LoS blockage zones themselves.

The pdfs of blocked and non-blocked intervals, $f_L(t;x)$ and $f_B(t;x)$, are conditioned on the distance between the UE and the AP. Deconditioning with the help of (14), we establish the pdfs of blocked and non-blocked intervals when associated with the i-th nearest mmWave AP in the form

$$f_{L,i}(t) = \int_0^\infty f_A(t;x)f_i(x)dx, f_{B,i}(t) = \int_0^\infty f_B(t;x)f_i(x)dx, \quad (31)$$

which can be calculated numerically.

C. Capacity Received from a Single AP

The UE capacity when associated with i-th AP is

$$E[R_i] = cB\log\left(1+P_{R,i}/[N_0+I]\right), \quad (32)$$

where $P_{R,i}$ is the received signal power from the i-th nearest AP, N_0 is the Johnson-Nyquist noise at the receiver, I is the aggregate interference, and c is the constant coefficient that accounts for any MCS imperfections. Due to the random distances involved, $P_{R,i}$ and I are also RVs.

The received power and the power of interference are thus

$$P_{R,i} = P_T G_T G_R A X_i^{-\gamma}, \quad I = P_T G_T G_R A \sum_{j=0}^{\infty} X_j^{-\gamma}, \quad (33)$$

where γ is the path loss exponent, X_i is the distance to the currently serving AP, and X_j are the distances to the interfering APs. It is important to note that in our considered scenario I is independent of the actual connectivity scheme. Hence, in this section, we characterize the interference part of the capacity function.

Observe that the capacity can be represented as a function of two RVs: the received signal power, P, and the aggregate interference, I. To produce the mean capacity, we employ Taylor expansion of the capacity function. The second-order Taylor expansion of bivariate function $f(x,y)$ around $\vec{\theta} = (\theta_x, \theta_0)$ is

$$f(x,y) = f(\vec{\theta}) + f'_x(\vec{\theta})(x-\theta_x) + f'_y(\vec{\theta})(x-\theta_y) + \\ + \frac{1}{2}f''_{xx}(\vec{\theta})(x-\theta_x)^2 + f''_{xy}(\vec{\theta})(x-\theta_x)(y-\theta_y) + \\ + \frac{1}{2}f''_{yy}(\vec{\theta})(y-\theta_y)^2 + O(n^2). \quad (34)$$

Considering the expansion around $\vec{\mu} = (\mu_P, \mu_I)$, we have

$$E[f(\vec{\mu})] \approx f(\vec{\mu}) + \frac{f''_{xx}(\vec{\mu})\sigma_P^2 + 2f''_{xy}K_{P,I} + f''_{yy}(\vec{\mu})\sigma_I^2}{2}, \quad (35)$$

where $K_{P,I}$ is the covariance between P and I, while σ_P^2 and σ_I^2 are the variances of P and I, respectively.

Writing down the capacity function as

$$R = f(x,y) = cB\log(1 + x/[N_0(B) + y]), \quad (36)$$

we calculate the required derivatives in the form

$$\begin{cases} f''_{xx}(x,y) = -\frac{Bc}{\ln 2(N_0+x+y)^2}, \\ f''_{xy}(x,y) = -\frac{Bc}{\ln 2(N_0+x+y)^2}, \\ f''_{yy}(x,y) = \frac{Bcx(2N_0+x+2y)}{\ln 2(N_0+y)^2(N_0+x+y)^2}. \end{cases} \quad (37)$$

Analyzing (35), we establish that in order to compute the mean capacity one requires (i) the first two moments of interference, (ii) the first moment of received signal energy, and (iii) the covariance between them. As one may observe, there is no dependence between the interference energy and the received energy, which implies that $K_{P,I} = 0$ and leads to an approximation for R as in (23).

To determine the moments of I, we identify a circular zone around the UE of interest with the radius of R_I, such that the mmWave APs located outside of it do not significantly contribute to the aggregate interference at the UE, i.e., their contribution remains under the noise floor of $N_0(B)$. The number of interferers located within the circle of radius R_I follows a Poisson distribution with the mean of $\lambda_B \pi R_I^2$. Hence, the raw moments of interference can be obtained by using the Campbell theorem for isotropic point processes as follows

$$E[I^n] = \int_{R_B}^{R_I} (P_T G_T G_R A x^{-\gamma})^n p_L(x) p_C(x) 2\lambda_A \pi x dx, \quad (38)$$

where $p_L(x)$ is the non-blockage probability, $p_C(x)$ is the probability that the transmit and receive antennas are directed such that the interferer contributes to the aggregate interference at the UE, and $Ax^{-\gamma}$ is its contribution.

The probability $p_L(x)$ is provided in (13). Consider now $p_C(x)$. Due to the properties of the Poisson process and noticing that $R_B << R_I$, the interfering APs are distributed near-uniformly within the circle of radius R_I. Therefore, the distances to them follow the same distribution. Taking this fact into account and recalling that the length of an arc with the angle of α for the circle of radius x is given by $x\alpha$, as well as assuming the independence of antenna orientations at the APs and the UE, we arrive at

$$p_C(x) = (\alpha_T x/2\pi x)(\alpha_R x/2\pi x) = (\alpha_T \alpha_R/4\pi^2), \quad (39)$$

which implies that $p_C(x)$ is independent of x.

Substituting $p_C(x)$ and $p_B(x)$ into (38), we express

$$E[I^n] = \int_{R_B}^{R_I} (P_T G_T G_R A x^{-\gamma})^n e^{-2x\lambda_B r_B \frac{h_B - h_U}{h_A - h_U}} \frac{\alpha_T \alpha_R}{4\pi^2} 2\lambda_A \pi x dx =$$
$$= \frac{(P_T G_T G_R A)^n \alpha_T \alpha_R \lambda_A}{2\pi} \Big[R_B^{2-n\gamma} \Gamma\left(n\gamma - 1, \frac{2(h_B - h_U) R_B^2 \lambda_B}{h_A - h_U}\right) -$$
$$- R_I^{2-n\gamma} \Gamma\left(n\gamma - 1, \frac{2(h_B - h_U) R_B R_I \lambda_B}{h_A - h_U}\right) \Big], \quad (40)$$

where $\Gamma(a,x)$ is incomplete Gamma function.

D. Ergodic Capacity for Connectivity Schemes

Dynamics of the mean received power captures the type of connectivity scheme and thus helps characterize its performance. Below, we calculate the mean received energy and estimate the ergodic capacity for the considered mmWave connectivity strategies. Time diagrams of the introduced connectivity strategies are detailed in Fig. 4.

1) Static, nearest AP: In this scheme, the UE is associated with its nearest AP and does not change the association point in case of outage. Using (14) with $i = 1$, the mean energy of the received signal can be written as

$$E[P_{R,1}] = P_T G_T G_R A \int_{R_B}^{\infty} 2\pi\lambda_A x e^{-\pi\lambda_A x^2} x^{-\gamma} dx =$$
$$= \Big(\pi R_B^{-\gamma} \pi^{\frac{\gamma}{2}-1} \Gamma\left(1 - \frac{\gamma}{2}\right) \left[\lambda_A^{\frac{\gamma}{2}} R_B^{\gamma} - \left(\lambda_A R_B^2\right)^{\frac{\gamma}{2}} \right] +$$
$$+ \pi\lambda_A R_B^{-\gamma} R_B^2 E_{\frac{\gamma}{2}}\left(\pi\lambda_A r_B^2\right) \Big) P_T G_T G_R A, \quad (41)$$

where $E_y(x)$ is an exponential integral function.

Let A_1 be the RV that denotes active session time when the UE does not experience outage conditions. Observe that the UE has no service not only during its blockage time but also during the time T_S when it performs beamsearching as the link changes its state from blocked to non-blocked. The beamsearching time may or may not be longer than the time in non-blocked state, which implies that the active session time A_1 does not coincide with the non-blocked time L_1. Denoting by w_1 the probability that L_1 is greater than T_S, we have

$$w_1 = Pr\{L_1 > T_S\} = \int_0^{\infty} f_{L_1 - T_S}(x) dx, \quad (42)$$

where $f_{L_1 - T_S}(x)$ is the distribution of the difference $L_1 - T_S$. Note that the linear transformation $L_1 - T_S$ results in a displacement of the density $f_{L_1}(x)$ over the OX axis. As one may notice, with the complementary probability of $1 - w_1$, the UE receives no service during a non-blocked period. With the probability of w_1, the conditional distribution for the duration of an active period when the UE receives service is

$$f_{A_1}(x) = \frac{f_{L-T_S}(x)}{1 - \int_0^{\infty} f_{L-T_S}(x) dx} = \frac{1}{1 - w_1} f_{L-T_S}(x), x > 0. \quad (43)$$

The capacity during active time is found by substituting (41) and (40) into (23). Applying the mean conditional active time $E[A_1]$, the conditional fraction of time that the mmWave link remains active is

$$p_{A,1} = \frac{E[A_1]}{E[L_1] + E[B_1]}, \quad (44)$$

which leads to ergodic capacity in the form of

$$C = w_1 p_{A,1} E[R_1] = w_1 \frac{E[R_1] E[A_1]}{E[L_1] + E[B_1]}. \quad (45)$$

2) Static, LoS AP: Consider now the case where the UE chooses its nearest AP such that it is currently in non-outage conditions. The probability that the AP i is thus selected is

$$q_i = p_{L,i} \prod_{j=1}^{i-1} (1 - p_{L,j}), \quad (46)$$

where $p_{L,i}$ is non-blockage probability for AP i in (10).

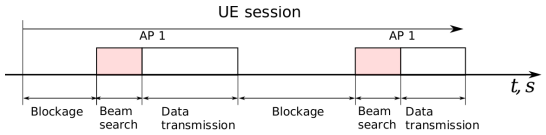

(a) Static nearest AP strategy

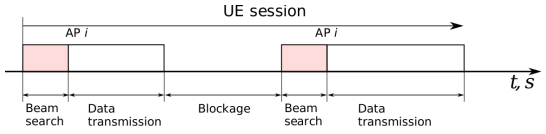

(b) Static LoS AP strategy

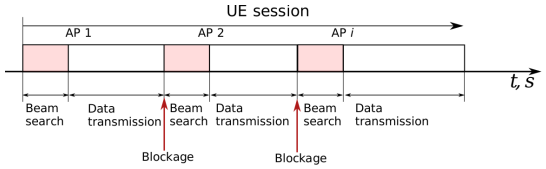

(c) Dynamic, $N = \infty$ strategy

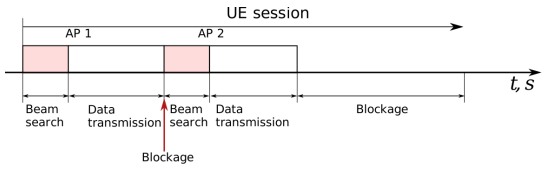

(d) Dynamic, finite N strategy

Fig. 4. Time diagrams of considered connectivity strategies.

The received signal strength from AP i is

$$E[P_{R,i}] = P_T G_T G_R A \int_{R_B}^{\infty} \frac{2(\pi\lambda)^i}{(i-1)!} x^{2i-1} e^{-\pi\lambda x^2} x^{-\gamma} dx = \\ = P_T G_T G_R A \frac{2(\pi\lambda_A)^i R_B^{2i-\gamma}}{(2i-\gamma)\Gamma(i)}, \quad (47)$$

which can be used to calculate the mean capacity $E[R_i]$ during active time when AP i is chosen by using (23).

Then, let A_i be the RVs denoting active session time when associated with AP i. Similarly, we define w_i as the probability that L_i (non-blockage time with AP i) is greater than T_S (beamsearching time). This probability is

$$w_i = Pr\{L_i > T_S\} = Pr\{L_i - T_S > 0\} = \int_0^{\infty} f_{L_i - T_S}(x) dx, \quad (48)$$

while the conditional pdf of link active time is

$$f_{A,i}(x) = \frac{f_{L_i - T_S}(x)}{1 - \int_0^{\infty} f_{L_i - T_S}(x) dx}, x > 0. \quad (49)$$

The fraction of time that a link remains active is

$$p_{A,i} = E[A_i]/(E[L_i] + E[B_i]), \quad (50)$$

which implies that the mean capacity when connected to AP i is a discrete RV with the probability mass function

$$\begin{cases} 0, & Pr\{L_i < T_S\} = 1 - w_i, \\ \frac{E[R_i]E[A_i]}{E[L_i]+E[B_i]}, & Pr\{L_i > T_S\} = w_i. \end{cases} \quad (51)$$

Weighting with the probabilities q_i, the ergodic capacity is finally produced as

$$C = \sum_{j=0}^{N} q_j w_j \frac{E[R_j]E[A_j]}{E[L_i] + E[B_j]}. \quad (52)$$

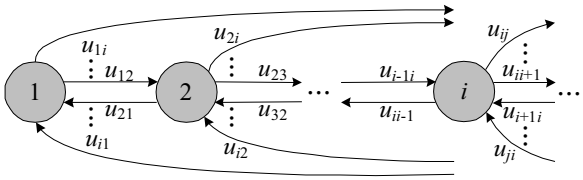

Fig. 5. Markov chain model of AP switching process with $N = \infty$.

The terms q_i, $i = 1, 2, \ldots$, in (46) approach 0 exponentially. Hence, the series for $E[C]$ in (52) converges as $i \to \infty$. In practical calculations, one should choose in (52) the number of APs, i, large enough, such that the contribution of $(i+1)$-th component is negligible.

3) Dynamic, $N = \infty$: In this case, whenever the UE that is currently associated with a certain mmWave AP is about to be blocked, it re-associates with its closest non-blocked AP. Observe that theoretically there always is an AP that resides in non-blocked state. Furthermore, the choice of a new AP to associate with depends on the current AP that enters the blocked state. Hence, the process of switching between the APs constitutes an irreducible aperiodic Markov chain as shown in Fig. 5, where state number i represents i-th nearest AP. The transition probabilities are thus

$$u_{ij} = p_{L,j} \prod_{k=1}^{i-1} (1 - p_{L,k}), \forall i, j = 1, 2, \ldots, i \neq j. \quad (53)$$

Let $\vec{\pi}$ be the steady-state probability vector of our introduced Markov chain. Observe that there is no closed-form solution for π. However, noticing that for all i u_{ij} in (53) decreases exponentially with j, in order to determine $\vec{\pi}$ we limit the state space of the chain to a sufficiently large value of N, such that $\sum_{j=1}^{N} u_{ij} \to 1$, $i = 1, 2, \ldots$. Introducing the transition probability matrix U, the steady-state vector is then obtained as a solution to $\vec{\pi}U = 1$, $\vec{\pi}\vec{e}^T = 1$, where $\vec{e}$ is the vector of ones with the size of N.

The pdf of the received signal power when associated with AP i is provided in (47). The RV determining the mean capacity when associated with AP i is calculated as

$$\begin{cases} 0, & Pr\{L_i < T_S\} = 1 - w_i, \\ \frac{E[R_i]E[A_i]}{E[L_i]}, & Pr\{L_i > T_S\} = w_i, \end{cases} \quad (54)$$

where $E[A_i]$ is available in (49).

Ultimately, the ergodic capacity is delivered by

$$C = \sum_{j=0}^{N} \pi_j w_j \frac{E[R_j]E[A_j]}{E[L_j]}. \quad (55)$$

4) Dynamic, finite N: When the UE may only associate with its nearest N APs, the connectivity pattern comprises two periods, T_1 and T_2. T_1 starts when the UE associates with its closest non-blocked AP for the first time after T_1 and ends when there are APs in non-blocked state. T_2 is the time duration when there are no APs in non-blocked state. Assuming independence of blockage processes at the APs, the CDF of the latter – conditioned on the event that the last AP

that the UE was associated with is the AP i – becomes

$$F_{T_2}(x;i) = 1 - [1 - F_{B_i}(x)] \prod_{j=1, i\neq i}^{N-1} [1 - F_{B_j^\star}(x)], \quad (56)$$

where B_i and $B_i^\star$ are the RVs denoting blockage and residual blockage periods, respectively, while $F_{B_i}(x)$ and $F_{B_j^\star}(x)$ are the corresponding CDFs. These are computed as in [44]

$$F_{B_j^\star}(t) = \int_0^\infty \frac{F_{B_i}(x+t) - F_{B,i}(t)}{t[1 - F_{B,i}(t)]} dt. \quad (57)$$

The probability that AP i is the last one that the UE was associated with before T_2 started, a_i, $i = 1,2,\ldots,N$, is

$$a_i = \prod_{j=1, j\neq i}^{N} (1 - p_{L,j}), i = 1,2,\ldots,N, \quad (58)$$

which leads to the CDF of T_2, $F_{T_2}(x) = a_i F_{T_2}(x;i)$.

Consider the period of time when the AP in non-blocked conditions is always available, T_1. Similarly to the dynamic connectivity case with $N = \infty$, the choice of AP to switch to depends on the current AP that changes its state from non-blocked to blocked. We model the switching process during T_1 by utilizing an absorbing Markov chain demonstrated in Fig. 6, where the state number i represents i-th nearest AP.

In contrast to the dynamic case with $N = \infty$, upon leaving each state the chain may absorb by indicating the start of T_2. To complete parametrization of the absorbing chain, one requires (i) matrix U that contains transition probabilities between the transient states $\{1,2,\ldots,N\}$, (ii) vector $\vec{u}$ that defines absorbing probabilities from each state, and (iii) vector $\vec{b}$ that specifies the initial state after the end of T_2. The elements of U are delivered by

$$u_{ij} = p_{L,j} \prod_{k=1}^{i-1} (1 - p_{L,k}), \forall i, j = 1,2,\ldots,N, i \neq j, \quad (59)$$

which implies that the elements of $\vec{u}$ are

$$u_i = 1 - \sum_{j=1, j\neq i}^{N} u_{ij}, i = 1,2,\ldots,N. \quad (60)$$

Producing an exact expression for the elements of $\vec{b}$ is cumbersome, since the AP that initiates the following T_1 depends on the last AP of the previous T_1. Disregarding this dependency, we establish that b_i has to be proportional to the mean duration of the blockage period, i.e.,

$$b_i = \frac{E[B_i]}{\sum_{j=1}^{N} E[B_j]}, i = 1,2,\ldots,N. \quad (61)$$

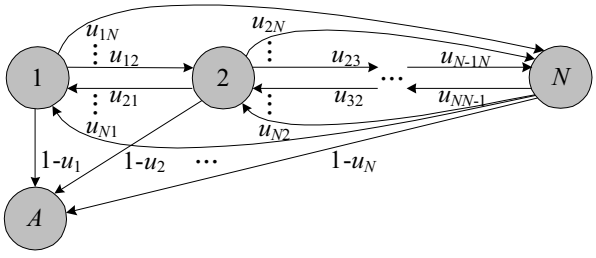

Fig. 6. Markov chain model of AP switching process with finite N.

TABLE IV
DEFAULT PARAMETERS FOR NUMERICAL ASSESSMENT.

Parameter	Value
Operating frequency	73 GHz
Height of AP, h_A	4 m
Height of blockers, h_B	1.7 m
Height of UE, h_U	1.5 m
Blocker radius, r_B	0.4 m
SNR blockage threshold, S_B	3 dB
Outage radius, R_B	97 m
Interference threshold, S_I	-174 dBm
Transmit power, P_T	0.2 W
Path loss exponent, γ	2.1
AP array, $H_{A,H} \times H_{A,V}$	64×4
UE array, $H_{U,H} \times H_{U,V}$	4×4
Bandwidth, B	0.59 GHz
AP/UE attenuation coefficients, A_A,A_U	1
Intensity of APs, λ_A	0.0001 units/m^2
Intensity of blockers, λ_B	0.5 units/m^2
Speed of blockers, v_B	1 m/s
Array switching time, δ	2 μs

Recall that the mean number of times that the chain visits a transient state is determined by the elements of fundamental matrix $D = (I - U)^{-1}$, while the mean number of steps before absorption is $D\vec{e}$ [45]. Hence, the mean capacity during T_1 is

$$E[C_{T_1}] = \sum_{j=1}^{N} \frac{1}{D\vec{e}} b_i d_{ij} w_j \frac{E[R_j]E[A_j]}{E[L_j]}. \quad (62)$$

Accounting for T_2, the ergodic capacity constitutes

$$C = \frac{E[T_1]}{E[T_1] + E[T_2]} \sum_{j=1}^{N} \frac{1}{D\vec{e}} b_i d_{ij} w_j \frac{E[R_j]E[A_j]}{E[L_j]}. \quad (63)$$

V. NUMERICAL ANALYSIS

In this section, we first conduct the accuracy assessment of the basic metrics within the developed model, which includes interference, SINR, and received power. Then, we proceed with a numerical analysis of introduced connectivity schemes and discuss the effects of system parameters in more detail. As there is a wide range of system parameters that affect the ergodic capacity, we primarily report on the behavior of aggregate interference, then analyze the connectivity schemes for the exhaustive search mechanism, characterize the impact of beamsearching mechanisms, and finally assess performance with different degrees of multi-connectivity. The default system parameters are summarized in Table V.

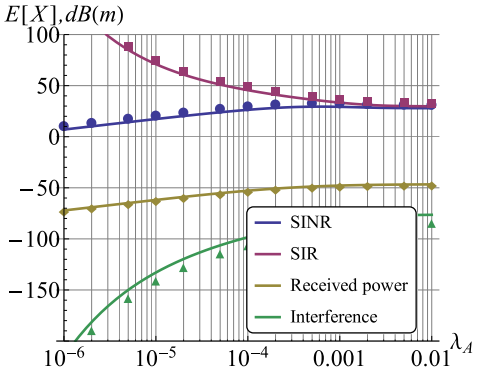

Fig. 7. Mean SINR, SIR, received power, and interference.

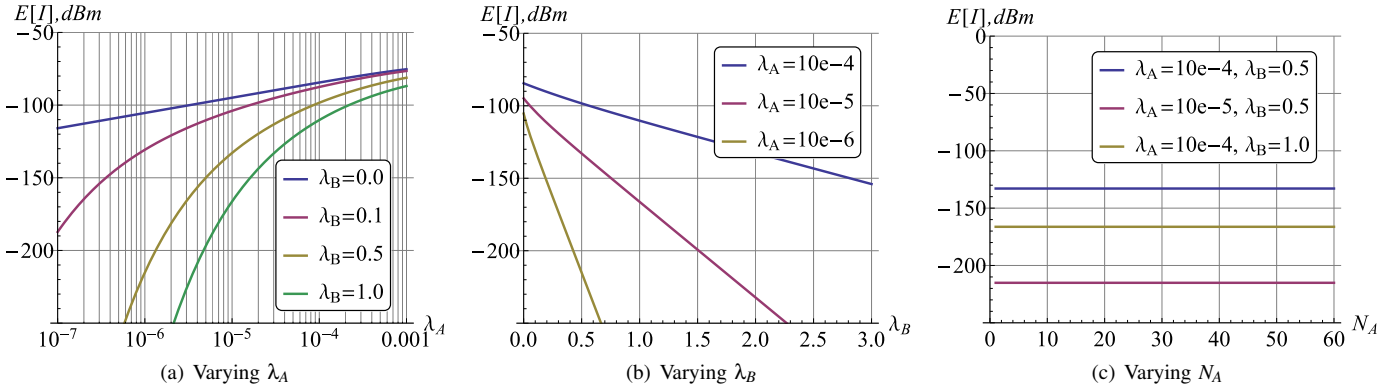

(a) Varying λ_A (b) Varying λ_B (c) Varying N_A

Fig. 8. Mean interference as function of blocker and AP intensities, λ_A, λ_B, and number of AP array elements, N_A.

Before using the developed analytical framework to illustrate the key numerical results, we first verify its accuracy by comparing the basic metrics against those obtained with computer simulations. To this aim, Fig. 7 illustrates the mean values of SINR, SIR, receiver signal power, and interference represented as functions of the mmWave AP intensity for the proposed mathematical model (lines) and system-level simulations (symbols). As one may observe, the developed interference modeling slightly overestimates the actual values of the mean interference, while the received signal power is approximated very tightly. As a result, both the mean SIR and SINR values are slightly overestimated as well. However, we notice that the actual difference is insignificant, thus implying that the basic metrics of interest are captured by the proposed modeling well enough. These observations allow us to reliably utilize the developed analytical framework in what follows.

A. Aggregate Interference

In our considered system, the aggregate interference is independent of the connectivity scheme and the beamsearching mechanism. However, since it directly affects the ergodic capacity, it is crucial to understand its behavior.

First, Fig. 8 illustrates the mean interference as a function of the blocker density, λ_B, AP density, λ_A, and the number of array elements at the AP, N_A, which are responsible for the horizontal directivity. Analyzing the results presented in Fig. 8(a), we observe that the mean interference increases as the density of APs becomes higher. Note that $\lambda_A = 10^{-5}$ corresponds to the mean inter-AP distance of approximately 150 m, while $\lambda_A = 10^{-3}$ relates to the distance of only 15 m. However, even for the latter, the mean interference remains low and reaches -75 dBm for the worst case of $\lambda_B = 0.0, \lambda_A = 0.001$. The effect of blockage is further illustrated in Fig. 8(b). As one may notice, the mean interference is a linearly decreasing function of λ_B for any λ_A. The reason is that higher values of λ_B decrease the probability for an interferer to contribute to the harmful energy at the UE.

The dependence of the mean interference on the number of antenna elements at the AP, N_A, is further demonstrated in Fig. 8(c). Importantly, the mean interference remains approximately constant for any value of N_A. This is because higher gains at the AP are compensated by smaller probabilities that the AP contributes to interference at the UE. Recall that the former increase proportionally to N_A, see Table III, while the latter decrease inversely proportional to N_A, and are approximated by $102/N_A$. These two terms in the expression for the mean interference in (40) compensate each other, thus leading to constant interference for any value of N_A.

B. Mean Conditional Capacity

The mean capacity with i-th nearest AP – conditioned on the event that these APs remain in non-blocked conditions – is shown in Fig. 9 for various values of the AP antenna arrays. Studying Fig. 9(a), one may notice that the effect of λ_A is not straightforward. Increasing the AP density from 10^{-6} to 10^{-5} and then to 10^{-4} naturally improves the mean capacity with i-th nearest AP. However, the highest capacity is provided in case of $\lambda_A = 10^{-4}$, which corresponds to the mean inter-AP distance of approximately 50 m. Increasing the density of APs further to 10^{-3} leads to a reduced capacity that is provided by i-th nearest AP. The explanation is that higher values of λ_A not only yield shorter distances to the APs but also mean closer interfering APs. Note that for a sufficiently high AP density of 0.001, which corresponds to the mean inter-AP distance of just 15 m, there is only a slight difference between the capacity levels offered by the first several APs. This is because the mean distances to these APs vary insignificantly due to conditioning on the fact that the UE is located outside of R_B.

It can also be noted that higher values of blocker intensity lead to more capacity as illustrated in Fig. 9(b) (assuming that active AP i is not blocked). This is a direct implication of the blockage phenomenon, where smaller values of blocker density lead to higher interference, see Fig. 8(b). Further, Fig. 9(c) suggests that a higher number of antenna elements at the AP increases the available capacity. Recall that the effect of N_A on the mean interference is negligible. Hence, the growth is mainly due to increasing gains at the APs.

Analyzing the data presented in Fig. 8(c), one can notice that increasing the number of antenna elements from 8 to 64 (thus, improving AP antenna gain from 8.57 to 17.59 dB) results in capacity growth of around 3 bit/s/Hz for all i-th nearest APs. Hence, on the one hand we may expect an increase in ergodic capacity as illustrated in Fig. 9(c). For small values of the number of antenna elements (up to approximately 30), we indeed observe this; however, enabling more antennas results in a gradual decrease of ergodic capacity. This is explained

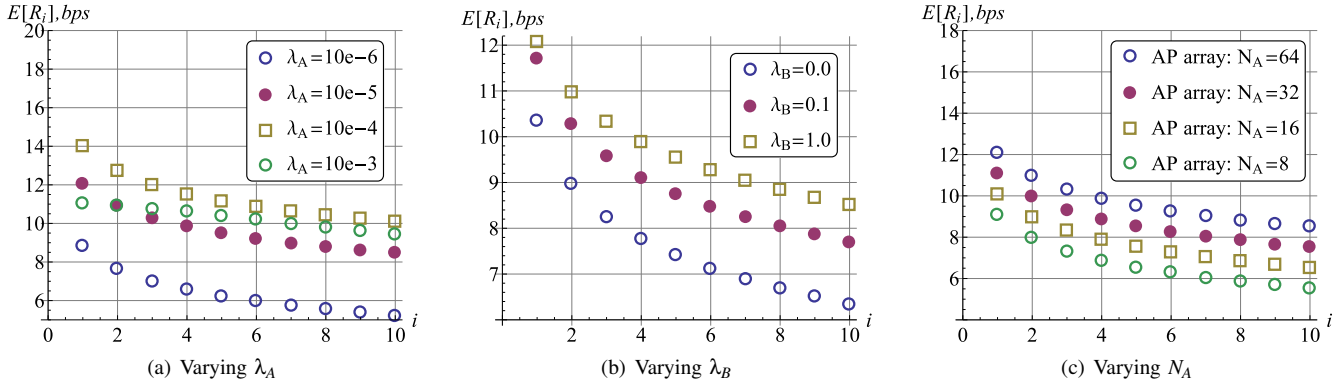

(a) Varying λ_A (b) Varying λ_B (c) Varying N_A

Fig. 9. Mean capacity when associated with AP i as function of blocker and AP densities, λ_A, λ_B, and number of AP array elements, N_A.

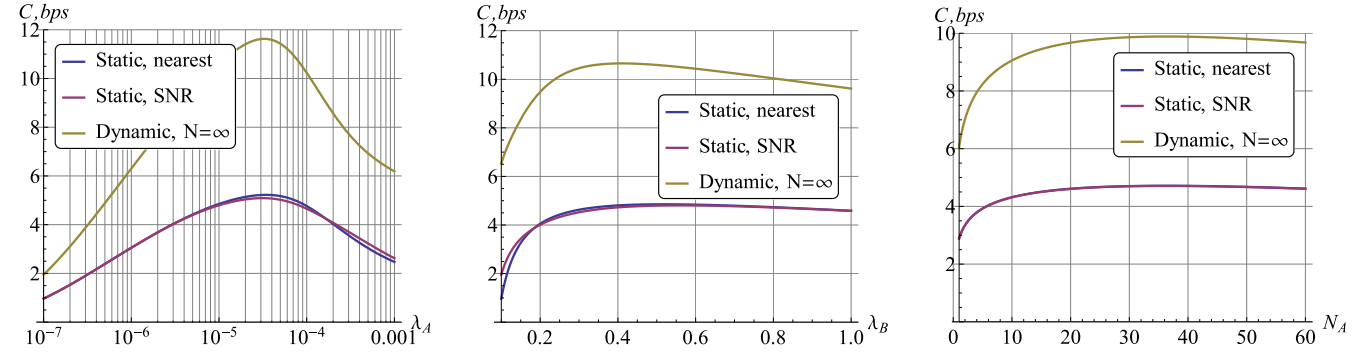

(a) Varying λ_A (b) Varying λ_B (c) Varying N_A

Fig. 10. Ergodic capacity for various connectivity schemes as function of blocker and AP intensities, λ_A, λ_B, and number of AP array elements, N_A.

by the fact that by increasing the number of antenna elements we also grow the beamsearching space. Having the array switching time fixed at $\delta = 2$ms in Fig. 9(c), the UE and APs have to spend more time for the above, and improved capacity no longer compensates for this. The effect is further exemplified in the next subsection, where we compare the operation of the two considered beamsearching schemes.

C. Exhaustive Beamsearching

After revealing the fundamental trade-offs that involve the intermediate metrics related to our parameter of interest, we now proceed with assessing the response of the ergodic capacity w.r.t. the system settings. We begin by considering the exhaustive search solution and compare the performance of two static schemes with that of a dynamic solution having an unlimited number of APs.

To this aim, Fig. 10 demonstrates the ergodic capacity for two static schemes and the dynamic alternative with $N = \infty$ as a function of blocker and AP densities, λ_A and λ_B, as well as the number of AP array elements, N_A. As expected, dynamic approach significantly outperforms its static counterparts for all values of system parameters. Further, the performance of two considered static schemes is similar. This is explained by the following two facts: (i) for any value of blocker density, non-blockage probability decreases exponentially with the AP index, which implies that the probability of choosing the nearest AP is high for static LoS strategy; and (ii) the mean conditional capacity provided by the APs does not vary considerably for several nearest APs, see Fig. 9.

Analyzing the dependence on λ_A further, we see that for a given set of system parameters there is an optimal inter-site distance (ISD) between the APs that maximizes the ergodic capacity for both static and dynamic connectivity strategies. The reason is that an increase in λ_A yields smaller distances to i-th AP and thus improves capacity that it delivers to the UE. However, at the same time, interference grows. An inflection point for the considered system parameters (see Table V) is $\approx 8 \cdot 10^4$, which corresponds to approximately 130 m. Note that the AP density maximizing the capacity coincides for both static and dynamic connectivity strategies.

It is curious to observe that the effect of blocker intensity on the ergodic capacity is complex as well, see Fig. 10(b). Recall that an increase in the density of blockers, λ_B, affects interference positively, see Fig. 8(b). However, at the same time, we observe an increased time spent in blocked state for the static schemes and growing frequency of transitions between the APs for the dynamic schemes. These latter effects negatively impact the ergodic capacity. As we notice in Fig. 10(b), the capacity first improves for all the connectivity strategies and then begins to degrade. In the first regime, the positive effect of decreased interference dominates the negative factors of increased blockage times and AP switching.

Finally, the response of the considered parameter to the number of antenna elements that determine directivity at the APs only marginally affects the ergodic capacity across the entire practical range of N_A, $10 - 64$. Nevertheless, for any set of input values, there is an optimal antenna directivity angle at the AP that maximizes the ergodic capacity. For the

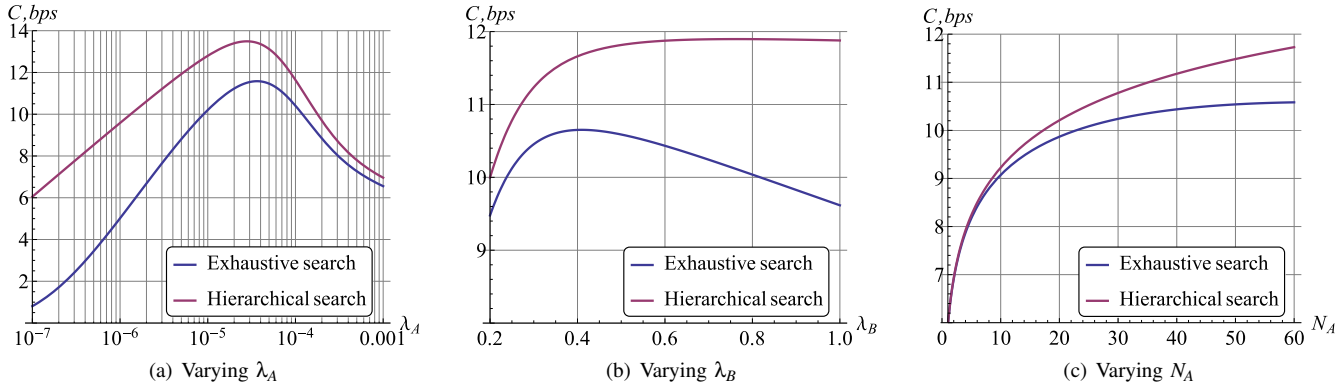

(a) Varying λ_A (b) Varying λ_B (c) Varying N_A

Fig. 11. Ergodic capacity for various beamsearching schemes as function of blocker and AP intensities, λ_A, λ_B, and number of AP array elements, N_A.

default parameters in Table V, the optimal number of antenna elements for a dynamic connectivity scheme is 32, which corresponds to the AP antenna directivity of $\alpha_T = 3.18°$.

D. Beamsearching Mechanisms

We now proceed with quantifying the effects of beamsearching mechanisms. To this end, Fig. 11 demonstrates the ergodic capacity for the dynamic connectivity scheme with $N = \infty$ and different beamsearching algorithms as a function of blocker and AP densities, λ_A and λ_B, as well as the number of AP array elements, N_A. As expected, enabling a more sophisticated beamsearching scheme leads to an increase in ergodic capacity. However, the quantitative effect depends on the environmental characteristics. Particularly, the difference is not drastic for very dense deployments, i.e., $\lambda_A > 10^{-4}$, which corresponds to approximately 50 m ISD.

For sparse deployments, the gain of applying advanced beamsearching is dramatic and reaches 4.5 bits/s/Hz. Furthermore, the gap between algorithms becomes larger as the density of blockers, λ_B, increases – as follows from Fig. 11(b). This is because the probability that non-blocked period is longer than beamsearching period grows slower than linear with λ_B for iterative beamsearching. Hence, as one may conclude, the ergodic capacity for the exhaustive search algorithm decreases much sooner as compared to its iterative alternative.

Analyzing data in Fig. 11(c), we finally note that the use of iterative beamsearching improves performance over the entire range of realistic antenna directivity values (up to approximately 1.59 beamwidth degree that corresponds to $N_A = 64$). This is in contrast to the exhaustive search scheme, which is characterized by slower growing ergodic capacity. Therefore, as expected, a larger number of antenna elements leads to an increase in ergodic capacity for both algorithms.

E. Degree of Dynamic Connectivity

In practice, maintaining associations with infinitely many APs is not feasible. Following the 3GPP considerations, multi-connectivity operation in mmWave systems is likely to be limited to several APs. In this subsection, we assess the performance of our dynamic scheme with the limited number of APs and compare it to the case of infinitely many APs.

First, Fig. 12 reports on the ergodic capacity for a dynamic scheme with different numbers of allowed AP associations, N, as a function of AP density, λ_A. A static scheme is also illustrated here for the sake of comparison. As one may observe, all dynamic profiles demonstrate a similar performance for lower values of λ_A (up to approximately $\lambda_A = 8 \cdot 10^{-4}$). Then, not only ergodic capacity starts to decrease for all the schemes, but also dual-connectivity mode begins to outperform the dynamic connectivity case with $N = 3$. The dynamic scheme with $N = \infty$ indicates the worst behavior out of all the considered dynamic schemes.

The discussed results may appear counter-intuitive, since maintaining more backup links should theoretically result in increased performance under dynamic blockage. This is indeed the case if beamsearching delays for backup links are disregarded (see e.g., [46]). However, as today's array switching time remains on the order of several microseconds, it is not negligible. During this time, the UE receives no service, which lowers the mean ergodic capacity. Comparing the capacity achieved with ideal switching time [46] against the results of our study, we observe that for all $N > 1$ the UE fails to achieve the theoretical upper bound on capacity.

A further growth of N yields a degradation in the achievable mean ergodic capacity. The reason is that for the considered system parameters the case of $N = 2$ suggests that the fraction of time when no non-blocked link is available remains very small. Hence, although an increase in N keeps reducing this value, the fraction of time that the UE dedicates for beamsearching with $N > 2$ becomes larger than the fraction of time when a non-blocked link is available for $N = 2$.

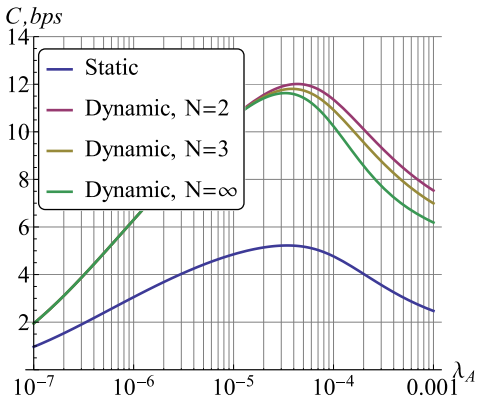

Fig. 12. Capacity for dynamic connectivity with finite N as function of λ_A.

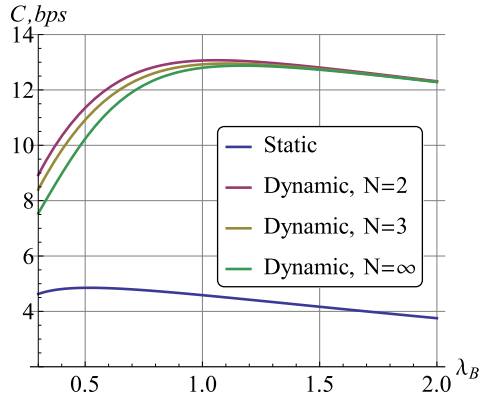

Fig. 13. Capacity for dynamic connectivity with finite N as function of λ_B.

The effect of λ_B on ergodic capacity with a finite degree of multi-connectivity, N, is displayed in Fig. 13. Similarly to the dependence on λ_A, dual-connectivity mode corresponds to the best performance out of all the considered connectivity strategies, while the dynamic scheme with $N = \infty$ becomes the worst out of all the dynamic cases. However, for extremely large values of λ_B, all of the dynamic schemes converge.

VI. Conclusions

In this work, we developed an analytical framework for the performance evaluation of connectivity strategies and beamsearching mechanisms in dense mmWave deployments. Our proposed methodology relates the UE ergodic capacity to important system parameters and environmental characteristics, which include AP density and height, blocker density and speed, number of antenna array elements, array switching time, degree of multi-connectivity, and connectivity strategies.

We further conducted a rigorous analysis of the system at hand by revealing a number of crucial qualitative and quantitative trade-offs. Particularly, we demonstrated that despite rather limited interference in the presence of highly directional antennas, its effect remains non-negligible and may impact the capacity actually delivered to users. Analyzing various types of connectivity mechanisms, we also confirmed that enabling multi-connectivity operation in mmWave systems dramatically improves the achievable capacity. However, an increase in the number of APs that the UE is associated with actually leads to worse performance, therefore making the dual-connectivity mode a preferred choice for mmWave system design.

This result allows to decrease the complexity of multi-connectivity systems and may further enable proactive beamsearching mechanisms, where the UE continuously tracks beams of the two nearest APs. For static approaches, we showed that the average and instantaneous SNR associations lead to approximately similar performance. Furthermore, for a given set of input parameters, there is an optimal density of APs that maximizes the ergodic capacity. Assessing performance of beamsearching mechanisms, we also revealed that an iterative beamsearching scheme improves UE capacity.

VII. Acknowledgement

This work was supported by the following Academy of Finland projects: Positioning-aided Reliably-connected Industrial Systems with Mobile mmWave Access (PRISMA) and Wireless Innovation between Finland and U.S. (WiFiUS).

References

[1] "M.2083: IMT vision - Framework and overall objectives of the future development of IMT for 2020 and beyond," ITU-R technical recommendation, 2015.
[2] "M.2376: Technical feasibility of IMT in bands above 6 GHz," ITU-R technical report, 2015.
[3] Y. Niu, Y. Li, D. Jin, L. Su, and A. Vasilakos V, "A survey of millimeter wave communications (mmWave) for 5G: opportunities and challenges," *Wireless Networks*, vol. 21, pp. 2657–2676, November 2015.
[4] M. Xiao *et al.*, "Millimeter wave communications for future mobile networks," *IEEE J. Sel. Areas Commun*, vol. 35, no. 9, pp. 1909–1935, 2017.
[5] 3GPP, "Study on channel model for frequencies from 0.5 to 100 GHz (Release 14)," 3GPP TR 38.901 V14.1.1, July 2017.
[6] M. Gapeyenko *et al.*, "On the temporal effects of mobile blockers in urban millimeter-wave cellular scenarios," *IEEE Trans. Veh. Technol.*, vol. 66, no. 11, pp. 10124–10138, 2017.
[7] W. Roh *et al.*, "Millimeter-wave beamforming as an enabling technology for 5G cellular communications: theoretical feasibility and prototype," *IEEE Commun. Mag.*, vol. 52, pp. 106–113, Feb. 2014.
[8] M. Giordani, M. Mezzavilla, and M. Zorzi, "Initial access in 5G mmwave cellular networks," *IEEE Commun. Mag.*, vol. 54, pp. 40–47, November 2016.
[9] S. Kutty and D. Sen, "Beamforming for millimeter wave communications: An inclusive survey," *IEEE Commun. Surveys Tuts.*, vol. 18, pp. 949–973, Secondquarter 2016.
[10] F. Maschietti, D. Gesbert, P. de Kerret, and H. Wymeersch, "Robust location-aided beam alignment in millimeter wave massive MIMO," pp. 1–7, December 2017.
[11] T. Nitsche, A. B. Flores, E. W. Knightly, and J. Widmer, "Steering with eyes closed: Mm-wave beam steering without in-band measurement," in *IEEE INFOCOM*, pp. 2416–2424, April 2015.
[12] N. Bhushan *et al.*, "Network densification: the dominant theme for wireless evolution into 5G," *IEEE Commun. Mag.*, vol. 52, pp. 82–89, February 2014.
[13] A. Osseiran *et al.*, "Scenarios for 5G mobile and wireless communications: the vision of the METIS project," *IEEE Commun. Mag.*, vol. 52, pp. 26–35, May 2014.
[14] V. Petrov *et al.*, "Dynamic multi-connectivity performance in ultra-dense urban mmWave deployments," *IEEE J. Sel. Areas Commun.*, vol. 35, pp. 2038–2055, September 2017.
[15] M. Gapeyenko *et al.*, "On the degree of multi-connectivity in 5G millimeter-wave cellular urban deployments," *IEEE Transactions on Vehicular Technology*, pp. 1–6, 2018.
[16] C. N. Barati *et al.*, "Initial access in millimeter wave cellular systems," *IEEE Trans. Wireless Commun.*, vol. 15, no. 12, pp. 7926–7940, 2016.
[17] J.-C. Guey, M.-P. Chang, C.-H. Yu, and C.-C. Su, "Modeling and evaluation of beam tracking in mobile millimeter wave communication," in *IEEE PIMRC*, pp. 775–780, 2015.
[18] M. Giordani, M. Mezzavilla, S. Rangan, and M. Zorzi, "Multi-connectivity in 5G mmWave cellular networks," in *MED-HOC-NET*, pp. 1–7, June 2016.
[19] V. Petrov, M. Komarov, D. Moltchanov, J. M. Jornet, and Y. Koucheryavy, "Interference analysis of EHF/THF communications systems with blocking and directional antennas," in *IEEE GLOBECOM*, pp. 1–7, 2016.
[20] V. Petrov, M. Komarov, D. Moltchanov, J. M. Jornet, and Y. Koucheryavy, "Interference and SINR in millimeter wave and terahertz communication systems with blocking and directional antennas," *IEEE Trans. Wireless Commun.*, vol. 16, pp. 1791–1808, March 2017.
[21] K. Venugopal and R. Heath, "Millimeter wave networked wearables in dense indoor environments," *IEEE Access*, vol. 4, pp. 1205–1221, 2016.
[22] K. Venugopal and R. Heath, "Location based performance model for indoor mmWave wearable communication," in *Proc. IEEE ICC*, 2016.
[23] M. Di Renzo, "Stochastic geometry modeling and analysis of multi-tier millimeter wave cellular networks," *IEEE Trans. Wireless Commun.*, vol. 14, no. 9, pp. 5038–5057, 2015.
[24] S. Singh, M. N. Kulkarni, A. Ghosh, and J. G. Andrews, "Tractable model for rate in self-backhauled millimeter wave cellular networks," *IEEE J. Sel. Areas Commun.*, vol. 33, no. 10, pp. 2196–2211, 2015.
[25] J. G. Andrews *et al.*, "What will 5G be?," *IEEE J. Sel. Areas Commun.*, vol. 32, no. 6, pp. 1065–1082, 2014.

[26] A. AlAmmouri, J. Andrews, and F. Baccelli, "SINR and throughput of dense cellular networks with stretched exponential path loss," *arXiv preprint arXiv:1703.08246*, March 2017.

[27] A. H. Jafari, J. Park, and R. W. Heath, "Analysis of interference mitigation in mmWave communications," in *IEEE ICC*, pp. 1–6, May 2017.

[28] A. Ravanshid *et al.*, "Multi-connectivity functional architectures in 5G," in *IEEE ICC*, pp. 187–192, 2016.

[29] S. Chandrashekar *et al.*, "5G multi-RAT multi-connectivity architecture," in *IEEE ICC*, pp. 180–186, 2016.

[30] M. Polese, M. Giordani, M. Mezzavilla, S. Rangan, and M. Zorzi, "Improved handover through dual connectivity in 5G mmWave mobile networks," *IEEE J. Sel. Areas Commun.*, vol. 35, pp. 2069–2084, September 2017.

[31] M. Mezzavilla, S. Goyal, S. Panwar, S. Rangan, and M. Zorzi, "An MDP model for optimal handover decisions in mmWave cellular networks," in *IEEE EuCNC)*, pp. 100–105, 2016.

[32] Y. Oguma, T. Nishio, K. Yamamoto, and M. Morikura, "Proactive handover based on human blockage prediction using RGB-D cameras for mmWave communications," *IEICE Trans. on Commun.*, vol. 99, no. 8, pp. 1734–1744, 2016.

[33] Y. Li, F. Baccelli, H. Dhillon, and J. Andrews, "Fitting determinantal point processes to macro base station deployments," in *IEEE GLOBECOM*, pp. 3641–3646, Dec. 2014.

[34] J. Kibiłda, B. Galkin, and L. A. DaSilva, "Modelling multi-operator base station deployment patterns in cellular networks," *IEEE Trans. Mobile Comput.*, vol. 15, pp. 3087–3099, December 2016.

[35] P. Nain, D. Towsley, B. Liu, and Z. Liu, "Properties of random direction models," in *IEEE INFOCOM*, vol. 3, pp. 1897–1907, March 2005.

[36] T. A. Thomas, H. C. Nguyen, G. R. MacCartney, and T. S. Rappaport, "3D mmwave channel model proposal," in *IEEE VTC*, pp. 1–6, September 2014.

[37] A. B. Constantine *et al.*, "Antenna theory: analysis and design," *Microstrip Antennas (third edition), John Wiley & Sons*, 2005.

[38] S. Singh, R. Mudumbai, and U. Madhow, "Interference analysis for highly directional 60-GHz mesh networks: The case for rethinking medium access control," *IEEE/ACM Trans. on Netw.*, vol. 19, pp. 1513–1527, October 2011.

[39] "Telecommunications and information exchange between systems local and metropolitan area networks – specific requirements. Part 11. Amendment 3," IEEE standard for information technology, 2012.

[40] S. Hur *et al.*, "Millimeter wave beamforming for wireless backhaul and access in small cell networks," *IEEE Trans. Commun.*, vol. 61, pp. 4391–4403, October 2013.

[41] D. Moltchanov, "Distance distributions in random networks," *Elsevier Ad Hoc Networks*, vol. 10, pp. 1146–1166, August 2012.

[42] R. Groenevelt, "Stochastic models for mobile ad hoc networks," PdD thesis, INRIA Sophia-Antipolis, 2005.

[43] D. R. Cox, *Renewal theory*. Methuen and Co ltd., 1970.

[44] S. Ross, *Introduction to probability models*. Academic Press, 2010.

[45] J. G. Kemeny, J. L. Snell, *et al.*, *Finite markov chains*, vol. 356. van Nostrand Princeton, NJ, 1960.

[46] D. Moltchanov, A. Ometov, S. Andreev, and Y. Koucheryavy, "Upper bound on capacity of 5G mmwave cellular with multi-connectivity capabilities," *Electronics Letters*, vol. 54, no. 11, pp. 724–726, 2018.

Mikhail Gerasimenko is a Researcher at Tampere University of Technology in the Laboratory of Electronics and Communications Engineering. Mikhail received Specialist degree from Saint-Petersburg University of Telecommunications in 2011. He obtained M.Sc. in 2013 and Ph.D. degree in 2018 from Tampere University of Technology. Mikhail started his academic career in 2011 and since then he appeared as (co-)author of multiple scientific journal and conference publications, as well as several patents. His main subjects of interest are wireless communications, machine-type communications, and heterogeneous networks.

Dmitri Moltchanov received the M.Sc. and Cand.Sc. degrees from the St. Petersburg State University of Telecommunications, Russia, in 2000 and 2003, respectively, and the Ph.D. degree from the Tampere University of Technology in 2006. Currently he is University Lecturer in with the Laboratory of Electronics and Communications Engineering, Tampere University of Technology, Finland. He has (co-)authored over 150 publications on wireless communications, heterogeneous networking, IoT applications, applied queuing theory. In his career he has taught more than 50 full courses on wireless and wired networking technologies. His current research interests include research and development of 5G/5G+ systems, ultra-reliable low-latency service, industrial IoT applications, mission-critical V2V/V2X systems and blockchain technologies.

Margarita Gapeyenko is a Ph.D. candidate at the Laboratory of Electronics and Communications Engineering at Tampere University of Technology, Finland. She earned her M.Sc. degree in Telecommunication Engineering from University of Vaasa, Finland, in 2014, and B.Sc. degree in Radio-Engineering, Electronics, and Telecommunications from Karaganda State Technical University, Kazakhstan, in 2012. Her research interests include mathematical analysis, performance evaluation, and optimization methods of future wireless networks, device-to-device communication, and 5G-grade heterogeneous networks.

Sergey Andreev is an Assistant Professor in the Laboratory of Electronics and Communications Engineering at Tampere University of Technology, Finland. He received the Specialist degree (2006) and the Cand.Sc. degree (2009) both from St. Petersburg State University of Aerospace Instrumentation, St. Petersburg, Russia, as well as the Ph.D. degree (2012) from Tampere University of Technology. Sergey (co-)authored more than 150 published research works on wireless communications, energy efficiency, heterogeneous networking, cooperative communications, and machine-to-machine applications.

Yevgeni Koucheryavy is a Full Professor in the Laboratory of Electronics and Communications Engineering of Tampere University of Technology (TUT), Finland. He received his Ph.D. degree (2004) from TUT. He is the author of numerous publications in the field of advanced wired and wireless networking and communications. His current research interests include various aspects in heterogeneous wireless communication networks and systems, the Internet of Things and its standardization, as well as nano-communications. He is Associate Technical Editor of IEEE Communications Magazine and Editor of IEEE Communications Surveys and Tutorials.